ResearchGate

See discussions, stats, and author profiles for this publication at: https://www.researchgate.net/publication/270411326

Identification of hydrothermal paleofluid pathways, the pathfinders in the exploration of mineral deposits: A case study from the Sukumaland Greenstone Belt, Lake Victoria Gold Fie…

Article *in* Advances in Space Research · December 2014

DOI: 10.1016/j.asr.2014.11.024

READS

131

3 authors, including:



Elisante Elisaimon Mshiu

University of Dar es Salaam

6 PUBLICATIONS **13** CITATIONS

SEE PROFILE



Glaesser Cornelia

Martin Luther University Halle-Wittenberg

93 PUBLICATIONS **243** CITATIONS

SEE PROFILE

Available from: Elisante Elisaimon Mshiu

Retrieved on: 25 July 2016

Available online at www.sciencedirect.com

ScienceDirect

Advances in Space Research 55 (2015) 1117–1133

ADVANCES IN SPACE RESEARCH (a COSPAR publication)

www.elsevier.com/locate/asr

Identification of hydrothermal paleofluid pathways, the pathfinders in the exploration of mineral deposits: A case study from the Sukumaland Greenstone Belt, Lake Victoria Gold Field, Tanzania

Elisante Elisaimon Mshiu [a,b,c,*], Cornelia Gläßer [b], Gregor Borg [a]

[a] *Economic Geology and Petrology Research Unit, Institute for Geosciences and Geography, Martin-Luther-University Halle-Wittenberg, Von-Seckendorff-Platz 3, D-06120 Halle, Germany*

[b] *Remote Sensing and Cartography, Institute for Geosciences and Geography, Martin-Luther-University Halle-Wittenberg, Von-Seckendorff-Platz 4, D-06120 Halle, Germany*

[c] *Geology Department, College of Natural and Applied Science, University of Dar Es Salaam, Tanzania*

Received 1 July 2014; received in revised form 24 October 2014; accepted 25 November 2014
Available online 2 December 2014

Abstract

Hydrothermal fluids play a key role in the process of metalliferous mineralization such as gold deposits. The modern exploration indicators for such deposits are tectonic structures and characteristic alteration minerals observed as detectable halos adjacent to mineral deposits. Tectonic fractures are the conduits to these hydrothermal fluids and thus control the spatial locations for the formation of mineral deposits. Along crustal structures, hydrothermal fluids commonly induce mineral alteration in the adjacent wall rocks depending on the physical–chemical conditions. These alteration patterns, which are the pathfinders for the proxies in the modern mineral exploration, can be detected by innovative application of combined remote sensing techniques. The study area has experienced intense tectonic deformations, which resulted to two major sets of structures, the NW–SE and NE–SW-trending structures. The knowledge-based analysis applied to SRTM data was useful in identifying crustal lineaments, which the above two set of structures, truncating lithological units of the Sukumaland Greenstone Belt were identified. The Feature Oriented Principal Component Selection (FPCS) together with the GIS functions applied to Landsat 7 ETM+ data, were useful to enhance signals from hydrothermal alteration minerals. Results have revealed that the Sukumaland Greenstone Belt is intensively fractured, in a systematic pattern, and has apparently been "injected" with large volumes of hydrothermal fluids. Both processes together have resulted in the systematic and structurally controlled hydrothermal alteration patterns. In this study linear alteration patches are interpreted to represent the hydrothermal paleofluid pathways. Alteration patches coincide spatially with regional and local tectonic structures and are consistent with major gold occurrences and gold mines. This study indicate that careful analysis of SRTM and Landsat ETM+ data can identify crustal lineaments, the likely hydrothermal paleofluid conduits, which may lead to the discovery of potential ore deposits.
© 2014 COSPAR. Published by Elsevier Ltd. All rights reserved.

Keywords: New approach; Hydrothermal pathways; Hydrothermal alteration; Mineral exploration

1. Introduction

The best new mineral exploration tools and approaches in the aspect of ideas and technology are argued to be the likely solution to the current high demand of raw materials. Multispectral satellite remote sensing data, mostly Landsat Thematic Mapper (TM) and Advanced Spaceborne Thermal Emission and Reflection Radiometer (ASTER) are

* Corresponding author at: Uvumbuzi Street, P.O. Box 35052, Dar Es salaam, Tanzania.
E-mail addresses: mshiutz@gmail.com (E.E. Mshiu), cornelia.glaesser@geo.uni-halle.de (C. Gläßer), gregor.borg@geo.uni-halle.de (G. Borg).

http://dx.doi.org/10.1016/j.asr.2014.11.024
0273-1177/© 2014 COSPAR. Published by Elsevier Ltd. All rights reserved.

currently common in mineral exploration. The data sets have been used in various researches, focused primarily on the identification of lithologies, minerals, and tectonic structures, through different signal enhancement techniques (Sadeghi et al., 2013; Carranza and Hale, 2002; Cloutis, 1996; Crósta and McMoore, 1989; Crósta et al., 2003; Fraser and Green, 1987; Goetz and Rowan, 1981; Hunt, 1977; Loughlin, 1991; Rowan and Mars, 2003;Sabins, 1999). In mineral exploration, remote sensing data have been used in identifying hydrothermal alteration minerals based on their proximity to mineralization. Crustal fractures being the main component in the hydrothermal systems play a major role in controlling the distribution of mineral deposits. It is because crustal fractures (e.g. faults and shear zones) are involved in carrying voluminous hydrothermal fluids during magmatism and in some parts they provide space for large volume of fluids to accumulate. This study was focused on using satellite remote sensing data to identify the crustal lineaments, which were likely used as hydrothermal fluid pathways during metallogenic events.

1.1. Wall rock alteration and fluid permeability

Hydrothermal wall rock alteration refers to fluid-induced mineralogical changes that alter the primary rock forming minerals adjacent to permeable fractures. The process occurs as a result of reactions between hydrothermal fluids and primary rock forming minerals, which commonly include the hydration of pre-existing minerals. The fluids are warm and contain variable amount of ligands (e.g. CO_2, H_2S, SO_2, CH_4, N_2), compounds (e.g. HCl and NaCl), metals and metal complexes such as Au and Au $(HS)^{2-}$ respectively. Fluid components under the changing physical and chemical conditions (e.g. pressure, temperature, pH, Eh), react with primary wall rock forming minerals to form secondary minerals, which are in equilibrium with the new geological environments. At the same time, the changes in physical and chemical conditions, as well as the ongoing alteration reactions, trigger the precipitation of other fluid components such as precious and base metals, which latter create mineral deposits. Hydrothermal alterations commonly create mineral zones within the host rock as a result of different stability conditions. These alteration zones normally exceed the spatial extent of mineralization and create cryptic hydrothermal alteration halos around veins and mineral deposits. The spatial extent of alteration minerals make the halos easier to recognize than the mineralization itself, this concept has been used in both historical and modern mineral exploration to search for mineral deposits (Pirajno, 2009).

Geological processes such as uplift and erosion are responsible for exposing the altered host rock on the surface whereby most of the primary alteration minerals are changed to new stable mineral phases, but some may remain stable for a long time under these atmospheric conditions (Fig. 1). Conditions such as low temperature and pressure, water, Eh, pH are catalysts to the reactions of these minerals. For example, hydrothermal anhydrite in veins may be hydrated to gypsum and subsequently dissolved in near surface environments. Hypogene hydrothermal minerals, e.g. sulfide and phyllosilicate are normally oxidized to Fe-oxide/hydroxide and clay minerals in near surface environments (e.g. Angélica et al., 1996;Klein and Day, 1994). Muscovite/sericite, chlorite, epidote, carbonates and silica (quartz) are amongst the hydrothermal minerals also found in the surface environments (Fig. 1). In remote sensing, some of these minerals, the infrared-active ones, from both primary and secondary alteration minerals, are used to identify areas, which may have likely been affected by hydrothermal alterations.

Rock porosity, permeability and reactivity are amongst the rock properties with significant roles in the diffusion of hydrothermal fluids in host rocks. Porosity and permeability control lateral infiltration of fluids into wall rocks. However, far more voluminous transportation of these fluids is through tectonic fractures, e.g. joints, faults as well as shear and breccia zones (Pirajno, 2009). These crustal fractures act as conduits and locally as funnels to large volume of fluids in hydrothermal systems. The above described role of tectonic fractures reveals a significant interdependence between fractures, hydrothermal fluids and hydrothermal alteration processes. As a consequence, crustal lineaments, which are commonly the remotely visible expressions of fault and shear zones, are the important traces of the hydrothermally altered areas.

1.2. Remote sensing data

Landsat TM data, both TM5 and TM7 are among the most used satellite multispectral remote sensing data in mineral exploration. The data sets have been used to locate target areas in the reconnaissance stages of exploration (e.g. Sadeghi et al., 2013; Crósta et al., 2003;Kruse et al., 2002). They are capable of identifying the areas rich in Fe-minerals and clay $\pm$ carbonate $\pm$ sulfate minerals. However, Landsat data are typically restricted to the identification of areas that may have likely been affected by hydrothermal alteration but are not capable of identifying the individual alteration minerals (Crósta et al., 2003).

Radar data is another remote sensing data set of which its use has recently brought a significant change in mapping the crustal lineaments (e.g. Masoud and Koike, 2011; Coltelli et al., 1996; Lowman, 1991;McFall and Singhroy, 1989). For example, shuttle radar topographical mission (SRTM) data have been used for extracting lineaments in different terrains (e.g. Kinabo et al., 2008; Masoud and Koike, 2011). Several processing techniques, established for enhancing signals from crustal lineaments, exist. These include different algorithms for automatic extraction of linear features, nowadays are embedded in different remote sensing software (Masoud and Koike, 2011). However, manual extraction of lineaments is also a common method

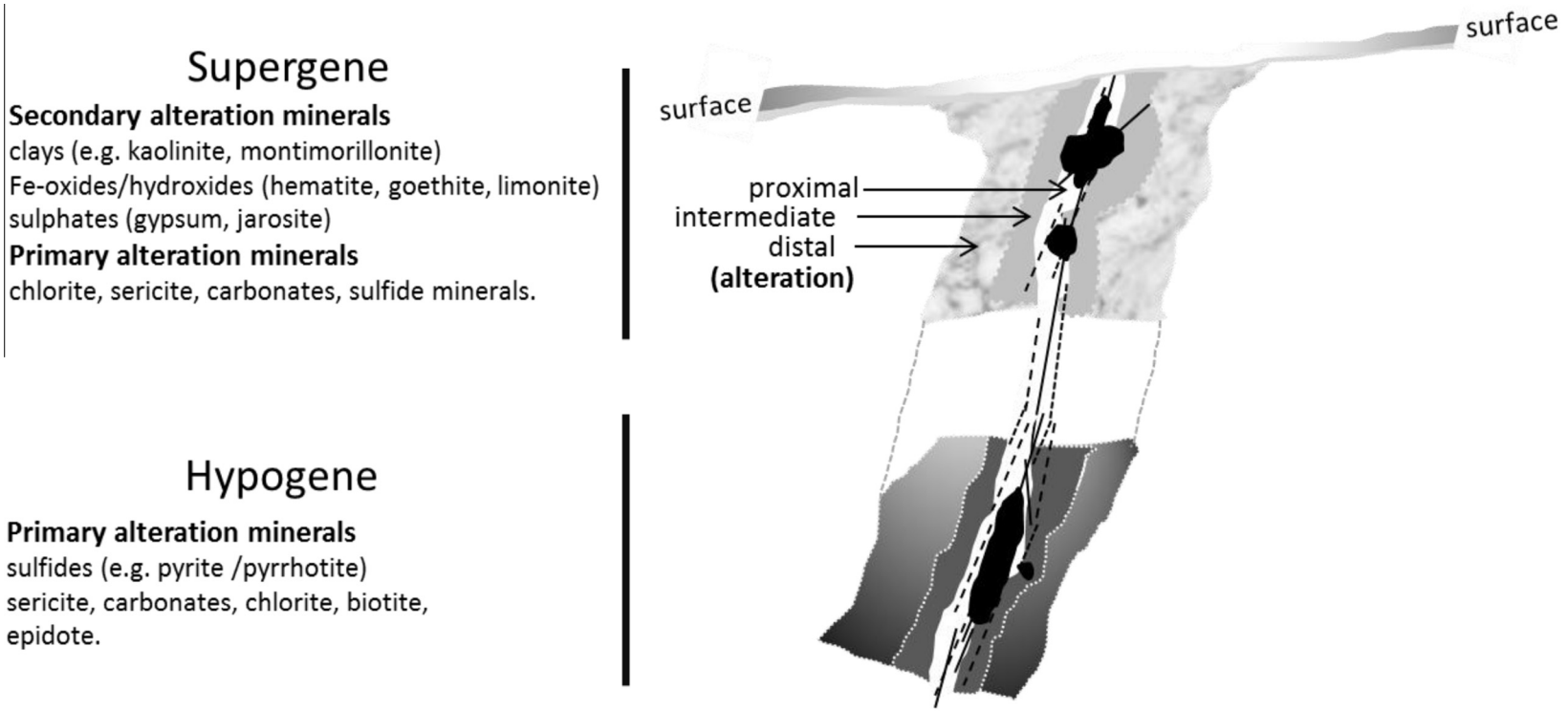


Fig. 1. A sketch outlining the distribution of some of the alteration minerals along crustal structures.

(Kumanan et al., 2011; Marghany and Hashim, 2010). Contrary to automatic algorithms, manual lineament extraction is the optional method to incorporate geological information from the study area during analysis. In this study, both SRTM and Landsat ETM+ data were used to identify lineaments or better crustal fractures, which were likely responsible in carrying hydrothermal fluids during metallogenic event(s).

2. The geology of the Sukumaland Greenstone Belt

The Sukumaland Greenstone Belt (SGB) is the largest among the eight Archaean greenstone belts in the Lake Victoria Gold Field (Fig. 2). The oval-shaped SGB is composed of Nyanzian mafic and felsic metavolcanic rocks, banded iron formations (BIF), metagranites and Kavirondian clastic metasediments

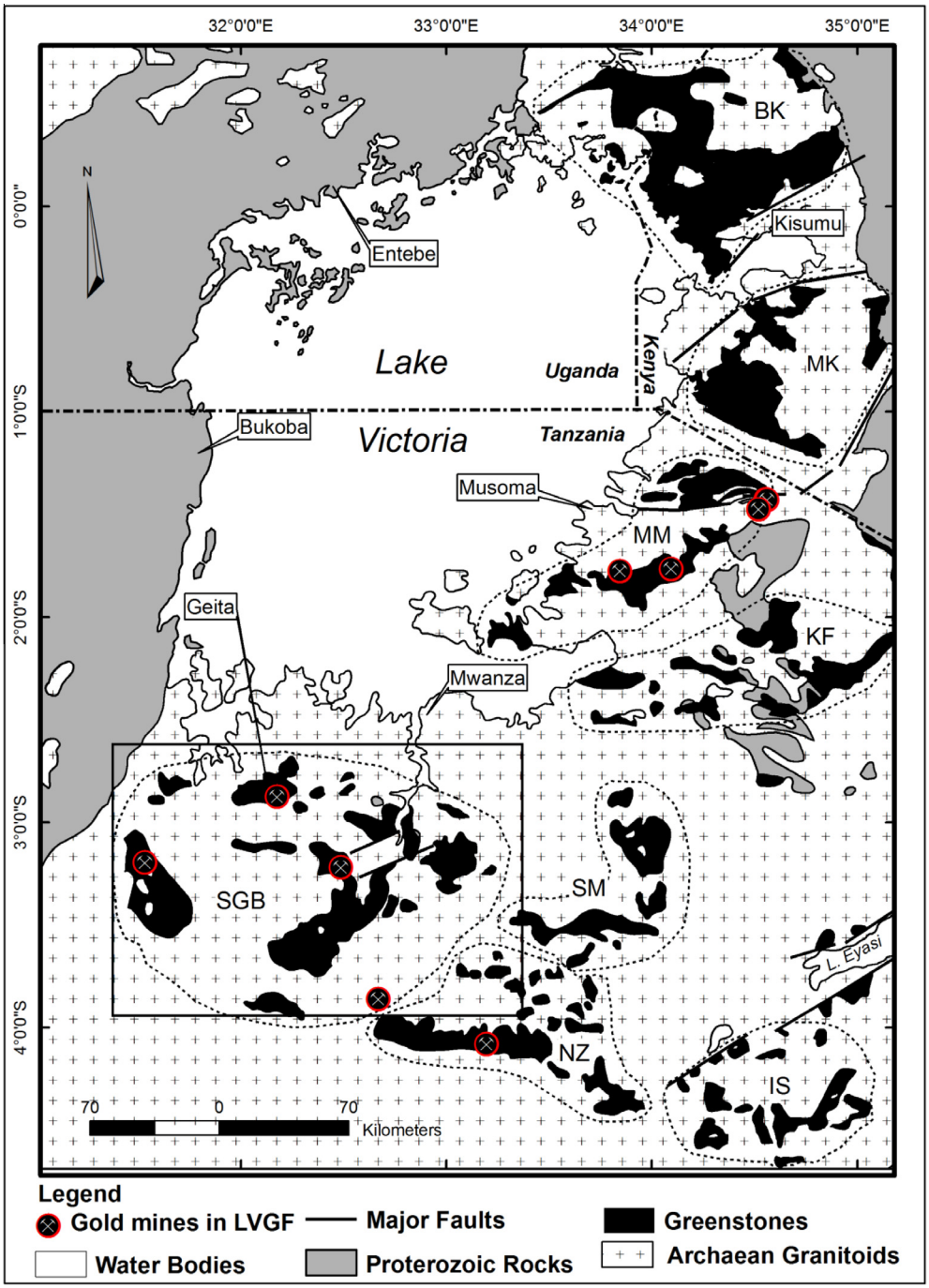


Fig. 2. A simplified geological map of the Lake Victoria Gold Field (LVGF) showing the greenstone belts and major gold mines. The greenstone belts are named, Sukumaland Greenstone Belt (SGB) enclosed in the box, Shinyanga–Malita Greenstone Belt (SM), and Kilimafedha Greenstone Belt (KM), Musoma–Mara Greenstone Belt (MM), Nzega Geenstone Belt (NZ), Iramba–Sekenke Greenstone Belt (IS), Migori–Kendu Greenstone Belt (MK), and Busia–Kakamega Greenstone Belt (BK). This map is a modification from Geological Survey of Tanganyika (1952), Barth (1990), Borg and Shackleton (1997), and Pinna et al., 2004.

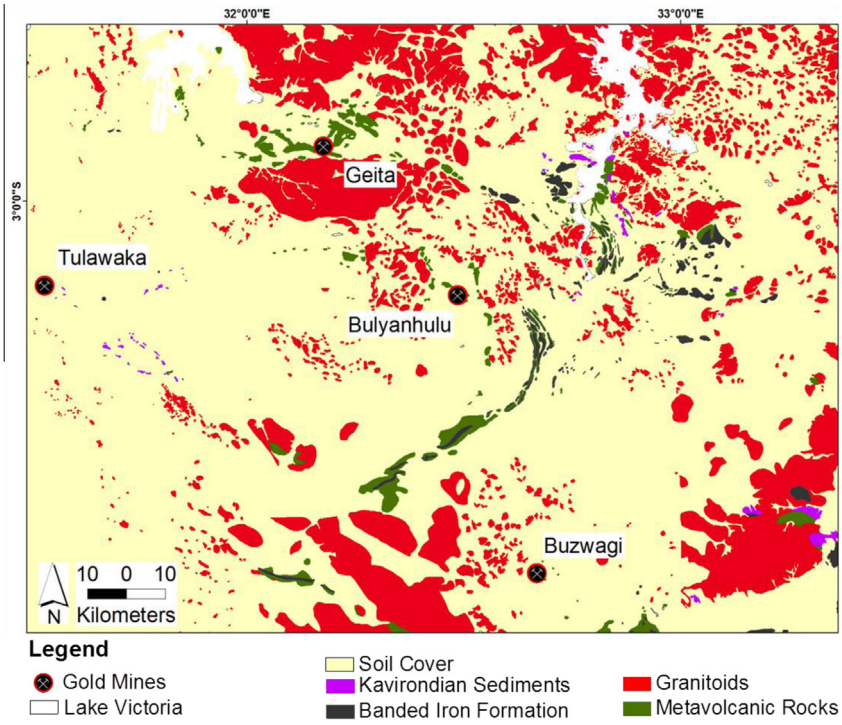


Fig. 3. Geological map of the SGB showing rock types and major gold mines.

(Borg and Shackleton, 1997;Cloutier et al., 2005; Manya, 2004; Manya and Maboko, 2008; Naylor, 1961). Mafic metavolcanics are mostly basaltic in composition, locally with pillow structures and occupy the lowest part of the stratigraphy. Felsic metavolcanic rocks mostly rhyolitic flows and tuffs overlay the basalts in the sequence. Chemical metasediments such as oxidic and sulfidic BIF occur subordinately as intercalations, predominantly above metarhyolites and tuffs (Borg, 1992; Borg and Shackleton, 1997). The top most part of the stratigraphy is covered by the clastic metasedimentary rocks, regionally the Kavirondian, which rest unconformably on the older rocks. They mostly comprise conglomerates, grits, and clastic quartzites; the conglomerates are compositionally mature and contain predominantly pebbles from the underlying BIF (Borg, 1992; Borg and Krogh, 1999; Maboko, 2001). Intermediate to mafic dykes and sills have intruded the whole Archaean sequence; selective weathering of these dykes made them easily detectable in the underground exposures in Geita gold deposit (Eberle, 1988). The two prominent dyke swarms in the study area are easily recognized in aeromagnetic maps, one trending N–S and the other SW–NE (Borg, 1994). These dykes are extensive and mark two periods of significant magmatic activity that took place within the extensional crustal stress regime in the region (Borg, 1994).

Granites and granodiorites occupy a large portion by volume of all rocks of the region (Fig. 3); this is typical for Archaean granite-greenstone terrains. They intrude and flank the metavolcanic rocks and in some places are reported to cause contact metamorphism and raise the metamorphic grade up to middle amphibolite facies. However, regional metamorphic grade of the SGB ranges from lower greenschist to upper greenschist facies (Borg and Shackleton, 1997; Naylor, 1961; Rammlmair et al., 1990). The absolute age of the oldest rocks in SGB, the metabasalts, is 2823 ± 44 Ma (Manya and maboko, 2003). Granitoids are relatively younger, a recent reported $^{207}Pb/^{206}Pb$ dating of the SGB post-orogenic granites (high-K) has revealed the age range between 2660 and 2620 Ma (Stanislav et al., 2014). BIF in the SGB were dated through the trachyandesitic units interbedded together with BIF in Geita; the absolute age of these units is 2699 ± 9 Ma (Borg, 1994). This age represents the youngest available age limit for the greenstone sequences in the area (Borg and Krogh, 1999). Metasediments are dated between 2475 Ma and 2680 Ma, where the 2475 Ma is reported to be the youngest age for the Kavirondian metasediments in the Archaean Tanzania Craton (Borg and Krogh, 1999; Cahen et al., 1984).

2.1. Structures and geotectonics

The Archaean Tanzania Craton, similar to other stable Cratons, has been affected by different tectonic forces, and as the outcome, a number of major and minor fault zones, shear zones, folds and dykes characterize the Archaean rocks in the Tanzania Craton. Based on the interpretation of a country-wide aero-geophysical survey, the area shows a significant number of linear structures (Barth, 1990), largely structural systems, differing from each other in strike. The N–S and WSW–ENE-trending systems were identified to be sets of intermediate and mafic dykes intruded during different magmatic events. Examples of these dykes are the Proterozoic and Archaean dykes reported in the SGB

(Borg and Krogh, 1999; Borg and Masolla, 1991). The NW–SE and SW–NE systems represent the two dominant sets of conjugate shear zones and faults. The other one is E–W-trending system, which reflects the orientation of rocks, striking along the direction of metavolcanics and BIF (e.g. Vos et al., 2009).

With reference to Borg (1992), Grantham et al. (1945) and Stockley (1948), two major deformational events, D_1 and D_2, have affected the area. D_1 resulted in the formation of isoclinal folds with steep to vertical axial planes and horizontal fold axes. Strike directions of D_1 followed the general trend of the greenstone rocks. D_2 produced prominent fold shapes with parasitic S- and Z-folds, flexures and kink folds plunging with moderate to relatively steep angles in different directions. These events are reported to be of regional N–S compressional nature, which the best examples are the folds found in Geita Gold Mine (Borg, 1992). The seemingly random pattern of fold axes has been suggested to be caused probably by the active forces of extensive diapiric granite emplacement (Borg, 1992). Structurally, the Kavirondian metasediments, occupying the top most part of the stratigraphy, are far simple than other rocks. Folding in Kavirondian rocks is generally open with little tectonic complexity. However, the general trend of Kavirondian folding is similar to that of the adjacent rocks and in most cases Kavirondian appears to have been infolded within other Archaean rocks (Harpum, 1970).

2.2. Mineralization

Gold mineralization is found in all rock types (Borg et al., 1990), though economic concentration is commonly found in greenstone rocks and in the edge of greenstones close to the contact with the surrounding granites. To date there is only one potential major gold mine (Buzwagi Gold Mine, Fig. 3) where economic concentration of gold is found predominantly in granites (Ikingura et al., 2010). Apart from greenstones and granites, other gold-hosting rocks are BIF and more rarely clastic sedimentary units, good examples for such deposits are the Geita Gold Mine in the SGB (SU, Fig. 2) and the Golden Pride Gold Mine in the Nzega greenstone belt (NZ) respectively (Fig. 2).

Mineralization is predominantly tectonically controlled whereby major fractures, shear zones, faults and veins were used to channel mineralized hydrothermal fluids from lower crustal sources to the upper crust, causing the formation of gold deposits in the ductile–brittle transition zone, these fractures also appear to have controlled the intrusion of the observed dyke swarms in the region (Barth, 1990; Borg, 1994). Gold mineralization follows a specific regional tectonic pattern, which can be largely observed through structural elements. It has been reported and is well known that NW–SE and NE–SW are the two dominant regional orientations of gold bearing structures in the region (e.g. Borg, 1991; Chamberlain, 2003). Areas with intense tectonic deformation are reported to have relatively high abundant gold (Borg, 1991). Other favorable locations for mineralization are areas where greenstones have been intercepted by faults or major shear structures and where intense folding and dykes have deformed the greenstones. From the observations made by a number exploration pioneers, large amount of gold is suggested to have been driven by late granitic magmatic event(s) (e.g. Borg, 1991).

Generally, mineral alteration related to gold mineralization is typified by carbonatisation and sericitisation; these alterations are reported to post-date the initial deformation that tilted the stratigraphy into its present attitudes (Chamberlain, 2003). However, carbonatisation is a conspicuous feature throughout the sequence (Barth, 1990; Rammlmair, 1991). Other alterations include silicification, chloritisation, ferruginisation, minor tourmalinisation, pyrophyllite, and sulfidation. A general paragenetic sequence of pyrite, pyrrhotite, chalcopyrite, arsenopyrite, galena, sphalerite, magnetite, ilmenite, rutile and hematite has been recorded for a number of sulphides bearing ores (e.g. Weiser, 1986).

The SGB is the leading greenstone belt for the number of major gold mine and gold production. The large number of gold mines and research works conducted in this area, mostly in Geita and Bulyanhulu gold mines, were the criteria made to select the SGB for this study. The previous research works were used as reference during analysis and interpretation.

3. Method and analysis

3.1. Lineament extraction from SRTM data

SRTM data is freely available similar to Landsat ETM+ data; the data set was collected through a radar system on board of the Space Shuttle Endeavor on 11th to 22nd February 2000. The system used two synthetic aperture radars, a C-band system (5.6 cm) and an X-band system (3.1 cm) (Farr and Kobrick, 2000). 1 arc data (SRTM-1, 30 m X-Y resolution) and 3 arc data (SRTM-3, 90 m X–Y resolution and ±30 m root mean square error accuracy) are the two types of SRTM data available. The later is available for the areas outside United States and is the one used for the extraction of geological lineaments in the SGB. The image used is a sub-scene within coordinates 2° 0′ 2″–3° 59′ 53″ S latitudes and 30° 59′ 51″– 33° 59′ 32″ E longitudes.

There are several algorithms for automatic identification of linear features from spatial data sets such as SRTM. In principal, the concept behind is edge-detection, in which spatial and morphological filters are the basic tools used during analysis. In this study, we opted to use manual identification and interpretation of lineaments, the reason behind is that it allows the user to include the geological information of the study area. The geological characteristics considered include the attitudes of the two major sets of crustal lineaments that characterize the SGB. The available geological data has simplified to a great extent the entire process of interpretation. The process was done after

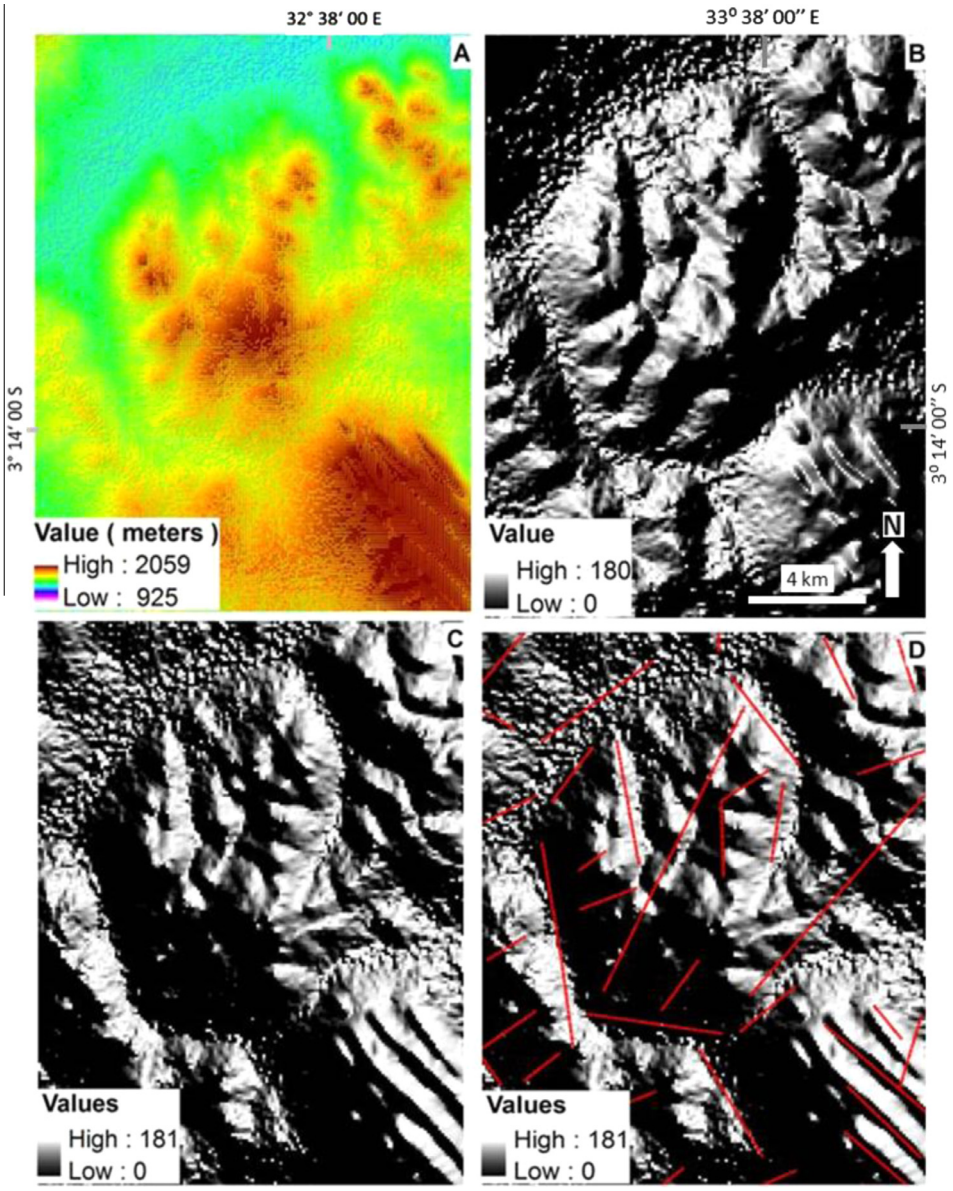


Fig. 4. Images from SRTM data, the area measures 18 km by 14 km. (**A**) Color stretching under histogram equalization (**B**) Hill shading in the direction 315° NW and 45° altitude (**C**) Hill shading in the direction 45° NE and 45° altitude (**D**) Image (**C**) overlain by lineaments extracted from SRTM data.

applying enhancement techniques, which were relevant for visual analysis. Enhancement methods such as color stretching under standard deviation with the use of sharp color ramps and shading were applied during the display of the SRTM image (Fig. 4A). Shading has also played a great role in enhancing lineaments. During shading, directional illumination was applied for the purpose of enhancing the two dominant sets of tectonic structures in the region. Illumination at 315° NW azimuth and 45° altitude was applied to enhance the NE–SW-trending tectonic lineaments whereas 045° NE azimuth and 45° altitude was applied to enhance the NW–SE-trending lineaments (Fig. 4B, Fig. 4C). The process of identification and extraction relied on abrupt change in color (tonal patterns), topographical scarps, and linear drainage patterns. On-screen digitization was the method used to extract the identified lineaments, in which one of the criteria used was to pick the visually recognizable lineaments with a length of at least 2 km.

Topographical and land use maps from the study area with a scale of 1:250,000 were used along side SRTM data during lineaments extraction to avoid picking the anthropogenic linear features such as roads, railways, and transmission lines. The accuracy of the extracted lineaments was calculated by overlaying the extracted lineaments with the documented tectonic fractures (e.g. faults, shear zones, joints) in geological maps.

3.2. Extraction of hydrothermal alterations from Landsat ETM+ data

Landsat TM comprises spectral data from three bands (bands 1, 2, and 3) in the VNIR region and three bands

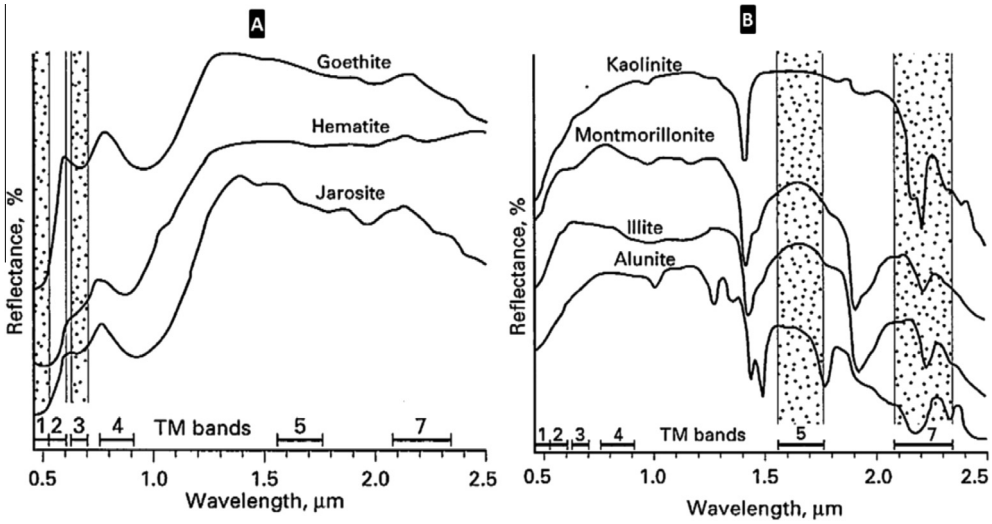


Fig. 5. Spectra graphs with wavelength positions for Landsat TM bands, (**A**) Fe-oxide/hydroxide minerals, (**B**) Clay minerals (Sabins, 1999).

Table 1
PCA results showing eigenvector statistics for Landsat ETM+ bands 1, 3, 4 and 5. The bands were selected to depict spectral responses from Fe-oxide/hydroxide minerals.

	PC1	PC2	PC3	PC4
Band1	0.4161	−0.7943	0.0383	**0.4410**
Band3	0.4345	−0.2232	−0.3958	**−0.7777**
Band4	0.3273	0.5401	0.8978	−0.2896
Band5	0.7287	−0.5624	−0.1892	0.3410

Table 2
PCA results showing eigenvector statistics from bands 1, 4, 5 and 7 of Landsat ETM+. The bands were selected for identifying spectral responses from clay ± carbonates ± sulphates minerals.

	PC1	PC2	PC3	PC4
Band1	0.3808	−0.9056	0.1416	−0.1216
Band4	0.3110	0.0646	−0.7271	0.6086
Band5	0.7042	0.3405	−0.2176	**−0.5838**
Band7	0.5122	0.2444	0.6356	**0.5235**

(bands 4, 5, and 7) in the SWIR region of the electromagnetic spectrum. Satellite images from Landsat ETM+ were used for analysis in this study. Bands 1-2-3-4-5-7 in Landsat ETM+ have 30 m spatial resolution. Band 6 is in the thermal infrared region of the spectrum with 60 m spatial resolution and the panchromatic band has 15 m resolution. The size of the Landsat ETM+ image is 183 km × 170 km for all bands (Global Land Cover Facility, 2012).

Landsat scenes, path 171 Row 062 and path 171 Row 063 used in this study, were acquired on 07th August, 2001 by Landsat ETM+ sensor. The selection of the scene was done purposely to obtain images captured from a dry season in Tanzania, specifically June to October. Images from dry season have experienced relatively little interference from vegetation signals, also water and clouds (Carranza and Hale, 2002). Prior to analysis, the images were geo-referenced and an appropriate projection (GCS_Arc_1960) for the study area was applied.

In the analysis of Landsat ETM+ data, bands from visible-near-infrared (VNIR) and shortwave- infrared (SWIR) regions were used for the identification of specific group of hydrothermal alteration minerals. In general, signal enhancement in the mapping of hydrothermal alteration minerals by Landsat ETM+ data, aims to identify clays ± carbonates ± sulphates minerals as one group and Fe-oxide/hydroxide minerals as another group (Sadeghi et al., 2013; Carranza and Hale, 2002; Crósta and McMoore, 1989; Crósta and Rabelo, 1993; Loughlin, 1991).

Fe-minerals are better identified using band 1 and 2 or 3 in Landsat ETM+ data and the other group with clay ± carbonates ± sulphates minerals are better extracted from band 5 and 7 (Fig. 5). However, spectral characteristics of the above two groups of minerals are also expressed by vegetation and thus create interference problems during analysis. Coincidentally, feature positions for minerals and vegetation in band 3 and 4 have opposite signs. Alteration minerals show high reflection in band 3 and absorption in band 4 whereas the vegetation has strong absorption in band 3 and high reflection in band 4. Therefore, the characteristics described above reveals band 3 and 4 can be used together with bands 1,2,5,7 during analysis to differentiate spectra from hydrothermal alteration mineral and those belonging to vegetation (Loughlin, 1991).

Principal component analysis (PCA) was a technique used in this study for the mapping of hydrothermally altered areas. The method applies a mathematical procedure that uses orthogonal matrix to convert a set of observations of possibly correlated variables into a set of values of linearly uncorrelated variables called principal components (Maćkiewicz and Ratajczak, 1993). The technique suppresses irradiant effects and enhances signals from target materials such as alteration minerals (Crósta et al., 2003). In our case, we used the modified feature-oriented

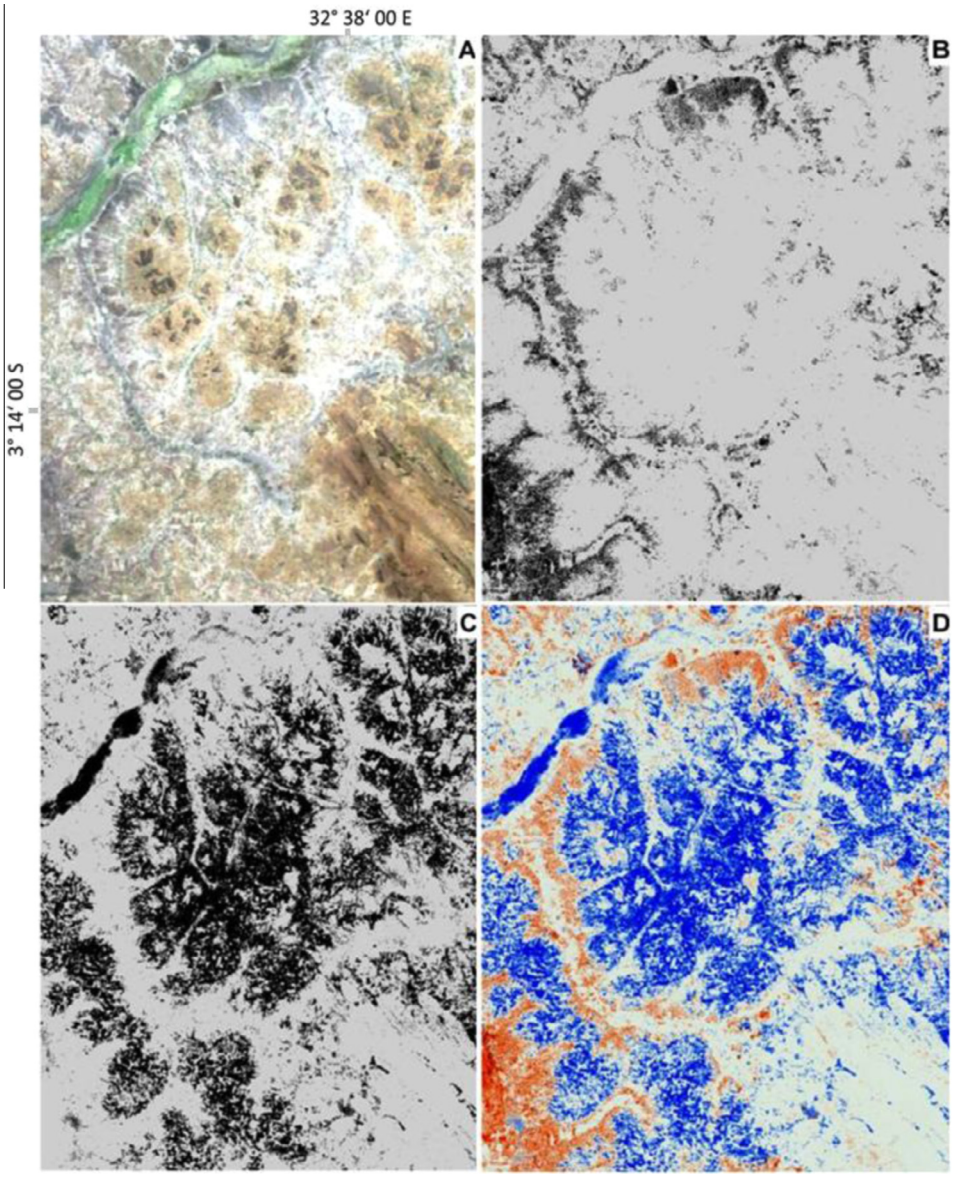


Fig. 6. Landsat ETM+ images, the area covered is 18 km by 14 km. (**A**) Composite image in true color from RGB bands 3:2:1 (**B**) PC4 for the Fe-oxide/hydroxide minerals (**C**) PC4 for the Fe-oxide/hydroxide minerals (**D**) RGB composite image.

principal component selection (FPCS) also known as Crósta technique (Crósta and McMoore, 1989; Loughlin, 1991), to map the hydrothermally altered areas in the SGB. The technique ensures the unwanted signals from materials such as vegetation are separated from geological/mineralogical target materials and collect them in a different principal component (PC). Crósta technique does not require much attention on pretreatments to suppress signals from vegetation since the unwanted signals will be collected in one of the resulting PCs, separate from the PC carrying target signals. Loughlin (1991) used Crósta technique on bands 1, 3, 4 and 5 to map spectral signatures related with Fe-oxide/hydroxide and bands 1, 4, 5 and 7 to map clay related mineral signals, and sometimes carbonates and sulphates. Spectra from these minerals will be mapped separately into either PC3 or PC4 whereas PC1 and PC2 collect signals from albedo and/or topographic information and contrast between VNIR and SWIR spectral regions respectively. The PCs, which carry target spectra will have high loadings in their respective diagnostic bands but with opposite signs (+ or −) (Loughlin, 1991).

In this study, vegetation signals are carried in PC3 with high loading from band 4 in both mineral groups. They have high positive loadings (0.8978) in the Fe-oxide/hydroxide group and high negative loadings (−0.7271) in the clay group (Table 1 and 2). Signals from Fe-oxide/hydroxide minerals are carried in PC4. The PC has moderate positive loading (0.4410) from band 1 and high negative loading (−0.7777) from band 3 (Table 1, bold numbers). The above observation indicates that signals from the target minerals will be represented by low (darker pixels) digital number (DN) values in PC4. Thus, PC4 had to be

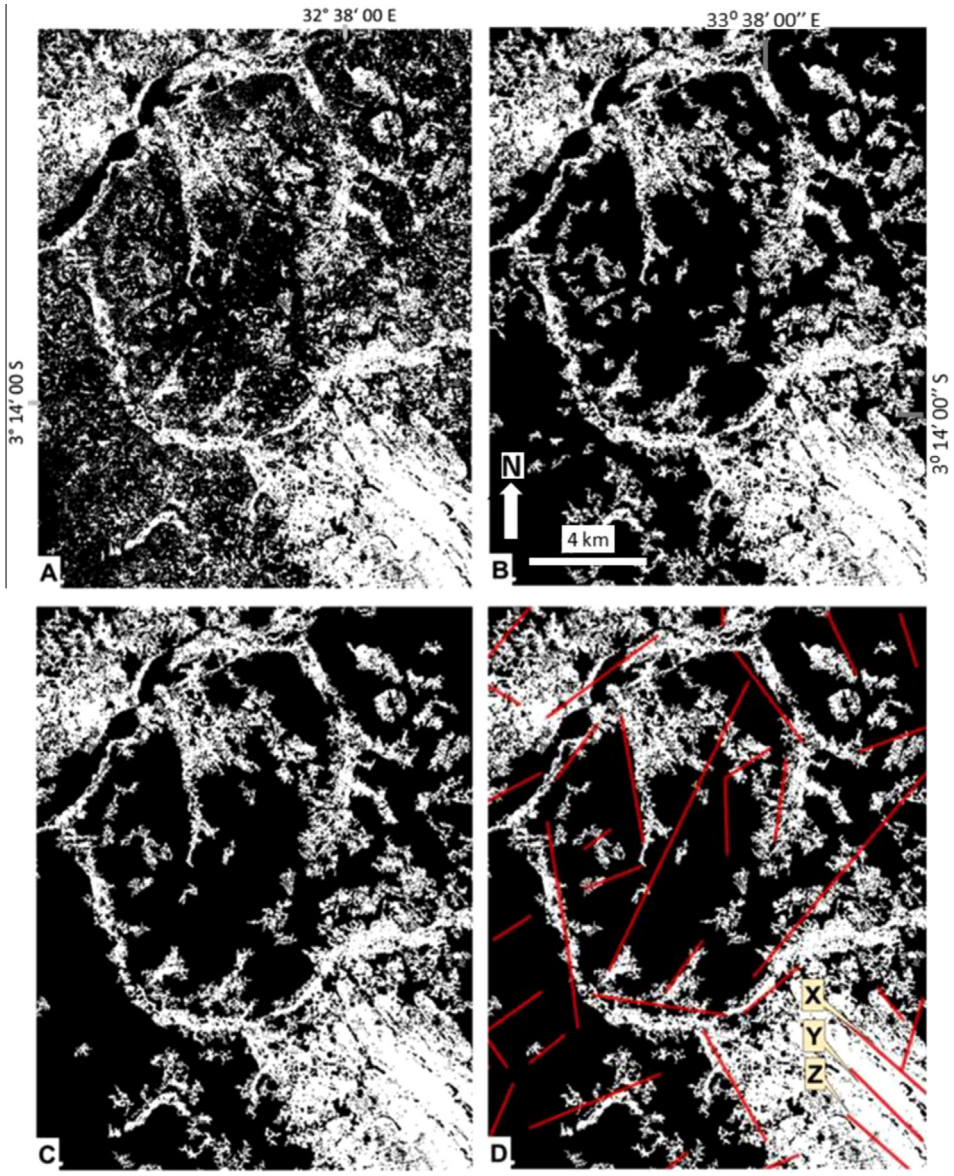


Fig. 7. Hydrothermal alteration images, the area covered is 18 km by 14 km. (**A**) Clumped pixels image but not sieved, (**B**) Sieved image with ⩽50 clumped pixels have been removed (**C**) Sieved image with ⩽100 clumped pixels have been removed (**D**) Image (**C**) overlain by SRTM lineaments.

negated by multiplying it with −1 to make pixels with Fe-oxide/hydroxide minerals displayed bright (Fig. 6B). Signals from clay group are similarly carried in PC4 (Table 2, bold numbers), the PC has high negative loading (−0.5838) from band 5 and high positive loading (0.5235) from band 7. Also PC4 had to be negated by multiplying it with -1 for the pixels from hydroxyl minerals to appear bright (Fig. 6C).

The resulting two images (Fig. 6B and C), the negated PC4s from both groups, were used to create a composite image in the RGB (Red, Green, and Blue) combination; a third image in the composite is the sum of the two resulting mineral images. In general, the RGB image displays mixed colors depending on the proportions contributed from pixels in each image. Pixels carrying hydrothermally alteration signals need to have high values from all mineral images. This means, effects of hydrothermal alteration is identified by pixels with high mineral concentration from both mineral groups. Therefore, pixels representing hydrothermally affected areas will appear white in RGB composite image (Fig. 6D).

3.3. Extraction of hydrothermal fluids paleochannels

Supervised classification was applied to the RGB image (Fig. 6D) to cluster pixels representing the hydrothermally altered areas and separate them from the unwanted pixels. In this process the light colored pixels were grouped together. The process was done through GIS recode function, which resulted to the suppression of the unwanted pixels by recoding them by value 0 and the target pixels were given value 1. The GIS function clumping was applied to the resulting image to polygonize the adjacent contiguous hydrothermal alteration pixels. The process resulted

to different shapes of the hydrothermally altered areas. The image was then subjected to sieving so as to remove the singly isolated and scattered pixels, those which appear unattached in relation to polygons of the clumped pixels. Sieving was performed repeatedly through varying the minimum number of pixels required to be removed to leave the altered areas in clearer shapes. 50 and 100 clumped pixels represent the sieved pixels in this study, which gave significant changes to the alteration image and in this study they stand as best examples for the technique used (Fig. 7B and C). With respect to spatial resolution of Landsat ETM+ data, areas represented by 50 and 100 pixels are equivalent to 0.045 km^2 and 0.09 km^2 respectively. The resulting "clean" image was overlaid with the extracted SRTM lineaments for interpretation (Fig. 7D).

4. Results and discussion

4.1. Crustal lineaments

The 90 m resolution SRTM data used in this study have proved to be suitable in the detection lineaments up to

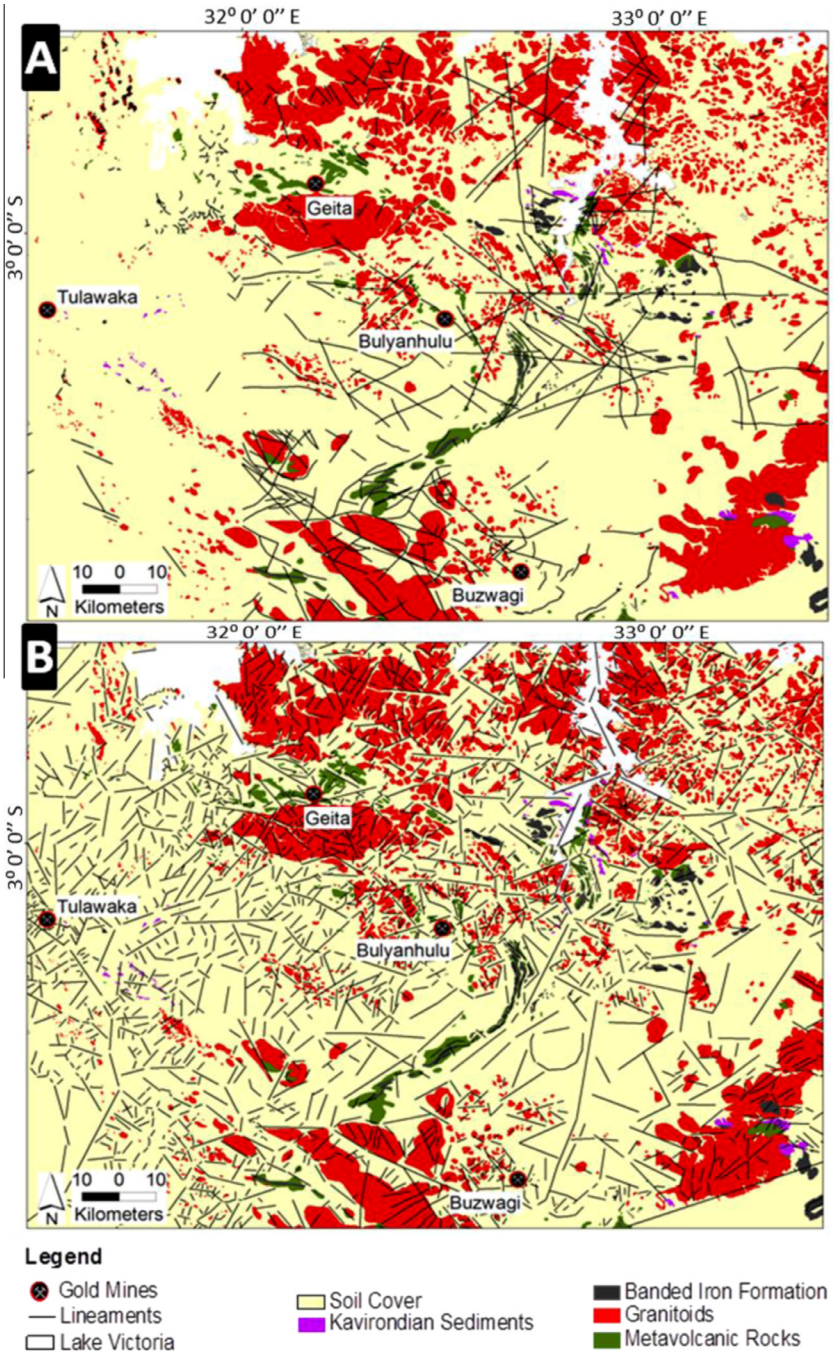


Fig. 8. The SGB geological map (**A**) The map overlaid with tectonic structures from geological maps, (**B**) The map overlaid with lineaments from SRTM data.

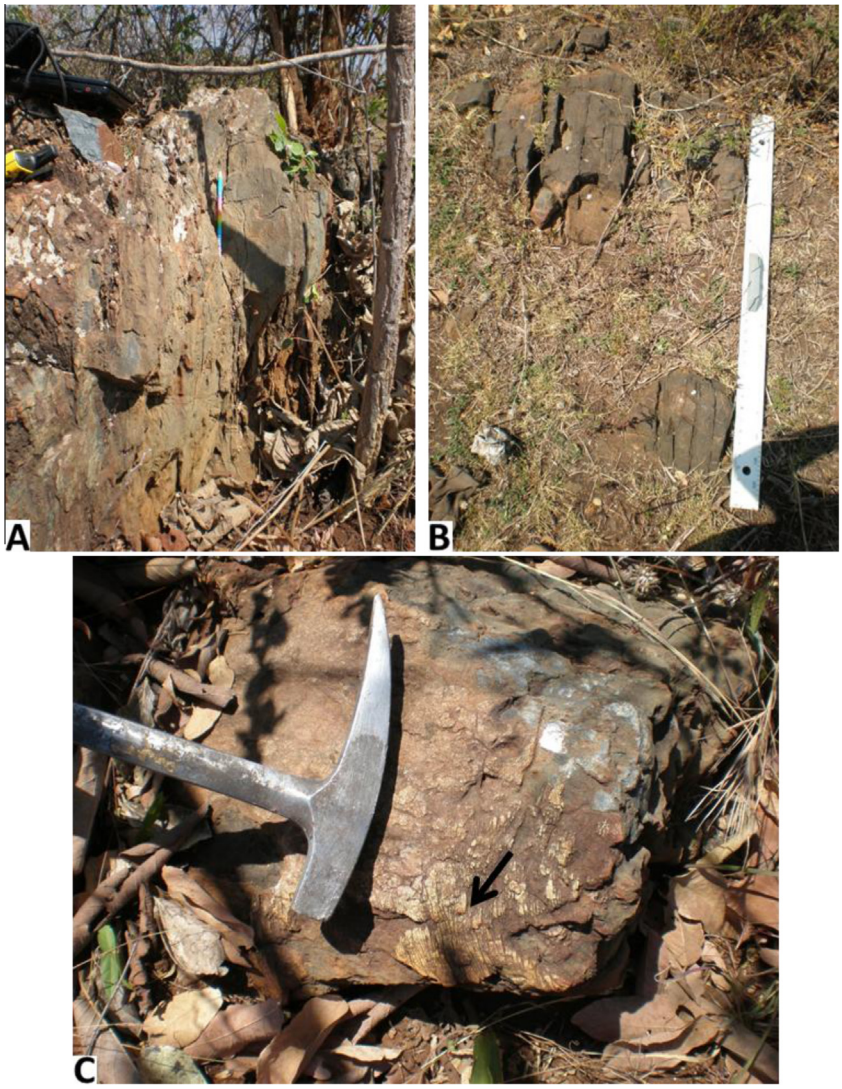


Fig. 9. Field pictures showing shearing features on outcrops, NW of Bulyanhulu Gold Mine. The shear zone is a continuation of a shear zone hosting mineralization in the Bulyanhulu gold deposit. (**A**) A plane of a shear, dipping vertical, (**B**) Outcrop with shear fractures, the ruler is 1 m, (**C**): Outcrop showing shearing surface, shown by the arrow.

<1 km long. This has led to a surprising large number of lineaments extracted. Prior to the present study the region had relatively few documented geological structures (Fig. 8A). In particular, areas covered with thick soils and/or forest had very few or no geological structures. The SRTM results from this study have revealed the study area have been intensively fractured (Fig. 8B). Results obtained are suggested to have been contributed much by the characteristics of the radar rays. It is generally difficult to identify a geological structure underneath a thick forest through aerial photo and sometimes by conventional field geological mapping, but properties exhibited by radar waves seems to overcome the obstacle. Characteristically, radar systems collect information on the surfaces of objects, for example, object heights. This means radar data such as data from SRTM, represent elevations of the object surfaces like tree canopies, building roofs and bare ground. However, SRTM data have not been reduced to bare Earth (Slater et al., 2006). The ability of the radar system to detect surface elevations, therefore, gives the possibility of detecting linear features on the Earth's surface. Features like linear topographical scarps or vertical offsets made by tectonic structures, for example, faults offsetting different rocks units, are identified through an abrupt change of elevation in SRTM data.

Results from this study have also revealed that forest characteristics to some extent have contributed in the identification of geological structures. Generally, a forest is dominated by a type of trees mostly with similar characteristics. For example, a forest has a common range of tree heights (e.g. Neumann et al., 2010). Based on the height factor, when these trees are located on a certain geological structure e.g. fault, the concealed fault dislocation will have a chance to be projected onto the forest canopy as abrupt height difference, and therefore the underneath structure can be detected by the radar sensor as a change in

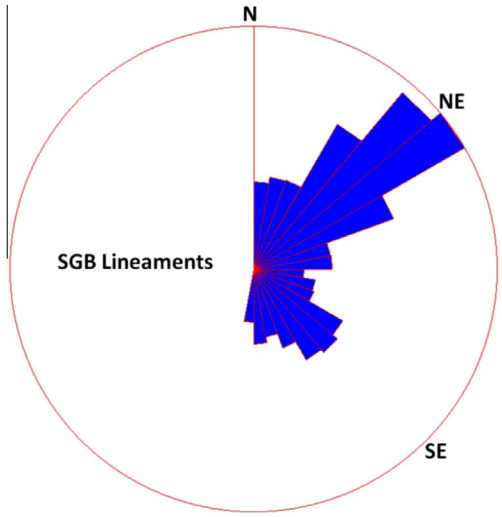


Fig. 10. A rose diagram for SRTM lineaments showing the two sets of lineaments, NE–SW and NW–SE-trending lineaments. The NE–SW set has relatively large number of lineaments compared to the NW–SE set as revealed by the size of histograms.

elevation. In this study, the mapped large number of lineaments, to the west of the study area, the densely forested part of the SGB, is suggested to have been successful due to the combined radar and forest characteristics.

The extracted lineaments from SRTM data have shown strong similarity with the known tectonic patterns of the region reported in Borg and Shackleton (1997). Hence, the study has revealed a far large number of crustal lineaments in the SGB. Field observation also confirmed the identified crustal lineaments, for example, the encountered indicators of shear zone to the NW of the Bulyanhulu Gold Mine (Fig. 9).

The NE–SW and NW–SE-trending lineaments, which are the dominant sets of lineaments in the SGB, are also revealed by the rose diagram (Fig. 10). There is another set trending E–W but it is insignificant in comparison to the above two sets. Calculations have revealed that 70% of the tectonic lineaments from geological maps are spatially coinciding with the extracted crustal lineaments from SRTM data. The presence of discrepant crustal structures in geological maps might be due to several factors. The source data where these structures were extracted and human error could be some of the factors. In some of the geological maps of the study area, tectonic structures are reported to have been obtained from interpretation of aeromagnetic data. Characteristically aeromagnetic data are capable of detecting crustal lineaments located several meters to hundreds of meters beneath the Earth's surface. Such deep-seated lineaments cannot be detected by radar systems and therefore cannot be identified in SRTM data. Other tectonic structures in these geological maps were extracted from other different data sets; including aerial photos and normal field geological mapping. Hence, the tectonic structures obtained from different data sources in the SGB geological maps, support the argument that there may be some discrepant lineaments from the two overlaid crustal lineament layers. These discrepant lineaments

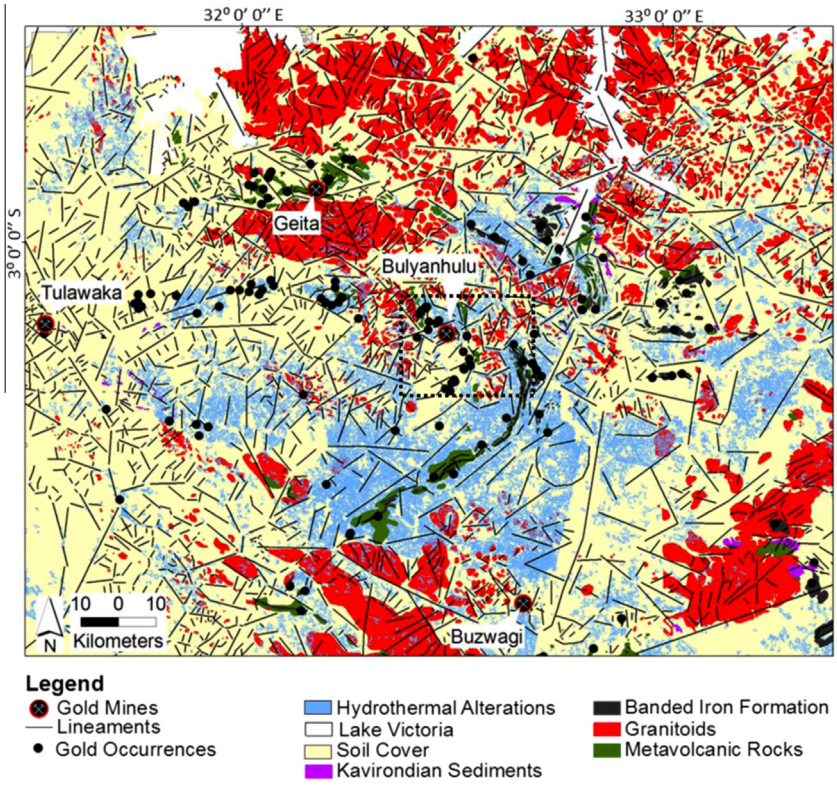


Fig. 11. The SGB geological map overlaid with SRTM lineaments, hydrothermal alterations and major gold occurrences. The area under frame is Bulyanhulu mining district, the representative area of this study.

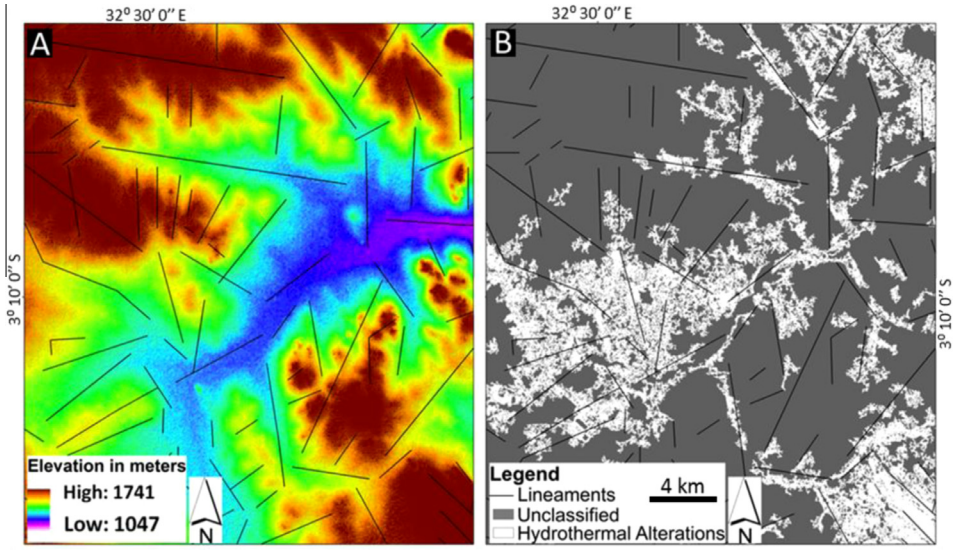


Fig. 12. Elevation versus distribution of hydrothermal alterations (**A**) Elevation image from SRTM data (**B**) Hydrothermal alteration image from Landsat ETM+ data.

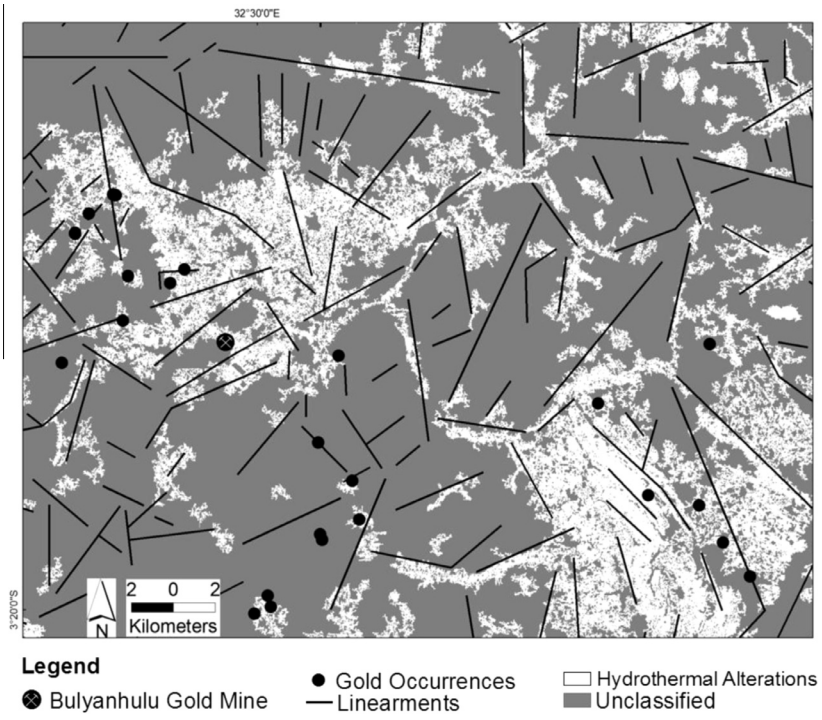


Fig. 13. Map of Bulyanhulu mining district showing the correlation between hydrothermal alterations, SRTM lineaments and gold occurrences. In this image clumped pixels $\leqslant 100$ have been removed.

include the remaining 30% uncorrelated structures from the SGB geological maps.

4.2. Hydrothermally altered areas in the Sukumaland Greenstone Belt

The results from Landsat ETM+ data shows the study area has been affected by hydrothermal alteration, in which the spatial distribution of the altered areas is controlled by structural patterns (Fig. 11). The areas affected by intensive alteration coincide with lineaments triple-junctions and areas where multi-lineaments are converging. The extent of hydrothermal alteration suggests the study area was strongly injected with hydrothermal fluids. As outcome, alteration process was not selective i.e. all rock types in the SGB have been affected by hydrothermal alteration.

However, the rock types such as metavolcanics, BIF, and clastic metasedimentary rocks shows to be relatively more affected (Fig. 11).

The altered areas were compared with SRTM elevation data to examine the possible influence of the accumulated soils in low elevation areas. Observation indicates no influence of soil interferences (preferential clay mineral accumulation) in low elevation areas as shown in Fig. 12. There is no correlation between the extent of hydrothermal alteration patches and low land areas, also hydrothermally altered areas are distributed throughout the elevation range. Effects of such interference would have been even more challenging if the distribution i.e. the shape and spatial extent of alteration areas were comparable to the distribution pattern of the lowland areas; results however show no such coincidence.

Most of the present known major gold deposits in the SGB (e.g. Bulyanhulu) as well as major gold occurrences are located within the hydrothermally altered areas (Fig. 13). For example, Bulyanhulu Gold Mine to the eastern part of the SGB is located within an alteration patch that trends in the NW–SE direction. The same is observed for the artisanal mining sites and major gold occurrences in the mining district. Most of the gold occurrences are located within the alteration patches, which are interpreted to have been formed as a result of the converging multi-lineaments (Fig. 13).

4.3. Hydrothermal paleofluid pathways

Crustal lineaments and the hydrothermally altered areas were extracted independently from two different data sets. The data sets have different spatial resolutions. Despite their differences, the overlay of their results has revealed correlation (Fig. 13). It is possible the linear alteration patches represent the former pathways for hydrothermal and potentially metalliferous fluids. These alteration patches are linear, straight and show similar patterns to both SRTM lineaments and crustal structures from SGB geological maps. Width of the mapped alteration patches ranges from around 300 m to 10 km; this variation is suggested to depend on the type of geological structure involved in the hydrothermal system. From the above case, the alteration patches associated with a shear zone will extend wider compared to the fault-related alteration patches.

Results also indicates for the two parallel crustal lineaments, where both were involved in hydrothermal fluid system, it is only one broad linear alteration patch that will be formed. The alteration patches of this kind show a strong intensity near the edges of the lineament and in the center area between the two lineaments. A particularly instructive example is the area between lineament Y and Z and between X and Y (Fig. 7D). The strong alteration intensity in the center area is suggested to be the meeting point of the alteration effects from both lineaments. For the case of parallel and closely spaced lineaments, alteration intensity is strong and uniform in the entire area between the two lineaments. However, the outside areas and areas away from the lineaments, alteration intensity is gradually decreasing, for example, the areas outside lineament X and Z (Fig. 7D).

Not all SRTM lineaments have spatial correlation with alteration patches; presence of such lineaments implies not all lineaments within the SGB were conduits to hydrothermal fluids (Fig. 13). Thus, we can distinguish the metallogenic potential from metallogenic barren lineaments. Likewise there are alteration patches with no spatial correlation with SRTM lineaments. Factors such as failure to identify these lineaments from SRTM data are suggested to contribute to the observed discrepancy. This could be due to lack of a topographical expression by the lineament itself, possibly due to its location far deep within the crust or a widespread surficial cover and weathering of the rocks cut by faults (Kinabo et al., 2008). Lineaments of such characters might not show their surface expression and can thus be difficult to identify them in the SRTM data.

5. Conclusions

The knowledge based analysis on SRTM data has extracted the two dominant sets of lineaments truncating the SGB rocks i.e. the NW–SE- and NE–SW-trending sets. These two sets of crustal lineaments are interpreted as a set of conjugate shears (e.g. Borg and Shackleton, 1997) of which the overall stress regime is assumed to be in the direction of σ_1 trending N–S and σ_3 in E–W direction. A large number of lineaments have been extracted, this reveals the SGB was intensively fractured, faulted and sheared, more than it was known before this study. The applied classification and GIS functions to Landsat 7 ETM+ data were powerful in identifying the hydrothermally altered areas and the correlation shown between alteration patches and crustal lineaments is a positive proof of the concept. The alteration patches, which stand as former hydrothermal fluid pathways in this study, coincide spatially with major gold mines and major gold occurrences in the study area. Areas indicated with high intensity of alteration are located adjacent to lineament triple junctions and areas where multiple lineaments are converging. These areas are suggested to have provided enough space for the accumulation of hydrothermal fluids. The ability to identify hydrothermal paleofluid pathways provide additional vector in mineral exploration since the paleofluid pathways could be used as pathfinder of the proxies of the hydrothermal related mineral deposits. The correlation shown between the mapped hydrothermal patches and major gold mines give a significant confidence to use this approach for the selection of target areas in mineral exploration.

Acknowledgements

The authors of this paper would like to thank the German Academic Exchange Service, i.e. Deutscher Akademischer Austauschdienst (DAAD), the Ministry of Education and Vocational Training in Tanzania (MoEVT), and the University of Dar-es-Salaam for the generous financial support of this project. We acknowledge the scientific discussions from members of the Economic Geology and Petrology Unit, and the Remote Sensing and Cartography Unit at Martin-Luther-Universität Halle-Wittenberg. The Global Land Cover Facility (GLCF) at the University of Maryland is acknowledged for provision of SRTM and Landsat ETM+ data. We are grateful for the anonymous reviewers for the constructive criticism, which led to the improvement of the manuscript. This paper forms part of a PhD project of one of the authors (**Elisante Elisaimon Mshiu**), which focused on using integrated data sets to study alteration minerals in areas around gold deposits in the Lake Victoria Gold Field (LVGF), Tanzania.

References

Angélica, R.S., da Costa, M.L., Pöllmann, H., 1996. Gold, wolframite, tourmaline-bearing laterized gossans in the Amazon region, Brasil.. J. Geochem. Explor. 57, 201–215.

Barth, H., 1990 (Provisional geological map of Lake Victoria Gold Fields, Tanzania, 1:500000). Geol. Jahrb. 72, 1–59.

Borg, G., 1991. Regional controls on the distribution of Au occurrences in the Sukumaland Greenstone Belt, NW Tanzania, IGCP Project No. 255 Conference, "Gold and Platinoids in Central Africa", Bujumbura, 11–13 September 1991, 3–4.

Borg, G., 1992 (New aspects on the lithostratigraphy and evolution of the Siga Hills, an Archaean granite greenstone terrain in NW-Tanzania). Z. für Angew. Geol. 38, 89–93.

Borg, G., 1994 (The Geita gold deposit, NW-Tanzania: Geology, ore petrology, geochemistry and timing of events). Geol. Jahrb., 545–595.

Borg, G., Lyatuu, D.R., Rammlmair, D., 1990. Genetic aspects of the Geita and Jubilee Reef Archaean BIF-hosted gold deposits, Tanzania, Geologische Rundschau, Stuttgart, 1990, v. 79, pp. 355–371.

Borg, G., Masolla, S.M.B., 1991. The lithotypes of the Sukumaland greenstone belt, NW-Tanzania: Geology and Genetic Evolution, IGCP No.255 final meeting "Gold and Platinoids in central Africa", Bunjumbura, 11–13, September 1991, Abstract volume, page 6.

Borg, G., Shackleton, R.M., 1997 (The Tanzania and NE Zaire Cratons). In: de Wit, M.J., Ashwal, L.D. (Eds.), Greenstone Belts. Clarendon Press, Oxford, pp. 608–619.

Borg, G., Krogh, T., 1999. Isotopic age data of single zircons from the Archaean Sukumaland Greenstone Belt Tanzania,. J. Afr Earth Sci. 29, 301–312.

Cahen, L., Snelling, N.J., Delhal, J., Vail, J.R., 1984 (Geochronology and Evolution of Africa). Clarendon Press, Oxford, page 512.

Carranza, E.J.M., Hale, M., 2002. Mineral imaging with Landsat Thematic Mapper data for hydrothermal alteration mapping in heavily vegetated terrain. Int. J. Remote Sens. 23, 4827–4852.

Chamberlain, C.M., 2003. Geology and genesis of the Bulyanhulu gold deposit, Sukumaland Greenstone Belt, Tanzania (DPhil. thesis). University of London and for Diploma of Imperial College of Science, Technology and Medicine, 401.

Cloutis, E.A., 1996. Hyperspectral geological remote sensing: evaluation of analytical techniques. Int. J. Remote Sens. 17, 2215–2242.

Coltelli, M., Fornaro, G., Franceschetti, G., Lanari, R., Migliaccio, M., Moreira, J.R., Papathanassiou, K.P., Puglisi, G., Riccio, D., Schwabisch, 1996. SIR-C/X-SIR multifrequency multipass interferometry. a new tool for geological interpretation. J. Geophys. Res. 101, 23127–23148.

Crósta, A. P., Rabelo, A. 1993. Assessing Landsat TM for hydrothermal alteration mapping in central–western Brazil, In: Proceedings of the Ninth Thematic Conference on Geologic Remote Sensing, Pasadena, California, USA, 8–11 February 1993, Proceedings, 1053–1061.

Crósta, A.P., Souza Filho, C.R., Azevedo, F., Brodie, C., 2003 (Targeting key alteration minerals in epithermal deposits in Patagonia, Argentina, using ASTER imagery and principal component analysis). Int. J. Remote Sens. 24, 4233–4240.

Crósta, A.P., McMoore, J. 1989. Enhancement of Landsat Thematic Mapper imagery for residual soil mapping in SW Minas Gerais State, Brazil, a prospecting case history in greenstone belt terrain: In: Seventh Thematic Conference on Remote Sensing for Exploration Geology, Calgary, Alberta, Canada, Proceedings, 1173–1187.

Cloutier, J., Stevenson, R.K., Bardoux, M., 2005. Nd isotopic, petrologic and geochemical investigation of the Tulawaka East gold deposit, Tanzania Craton. Precambrian Res. 109, 257–291.

Eberle, D., 1988. Basic Geophysical Aspects of Gold Prospection in Nyanzian Greenstone Belts of Tanzania: Tanzania-German Technical Cooperation, BRG internal report, Archaive No. 101791, Hannover, 86 pages.

Farr, T.G., Kobrick, M., 2000 (Shuttle radar topography mission produces a wealth of data, EOS Transactions). Am. Geophys. Union 81, 583–585.

Fraser, S.J., Green, A.A., 1987. A software defoliant for geological analysis of band ratios. Int. J. Remote Sens. 8, 525–532.

Geological Survey Of Tanganyika., 1:2000, 000 Geological map of East Africa, Government Printer, Dar es Salaam, 1952.

Goetz, A.F.H., Rowan, L.C., 1981. Geological remote sensing. Science 211, 781–791.

Global Land Cover Facility., Landsat Imagery, Overview, Landsat, (http://glcf.umd.edu/data/landsat/), 2012.

Grantham, D.R., Temperley, B.N., McConnell, R.B., 1945. Explanation of the geology of degree sheet No. 17 (Kahama). Geol. Surv. Tanganyika Bull. 15, 1–32.

Harpum, J.R., 1970. Summary of the geology of Tanganyika; part V, structural and geotectonics of the Precambrium. Geol. Surv. Tanganyika 1, 6–9.

Hunt, G.R., 1977. Spectral signatures of particulate minerals in the visible and near-infrared. Geophysics 42, 501–513.

Ikingura, J.R., Mutakyahwa, M.K.D., Marobhe, I.M., Manya, S., Kazimoto, E., Kasanzu, C., Mshiu, E.E., 2010. Atlas of Gold Deposits in Tanzania. A Book. University of Dar es Salaam and Barrick gold limited, 94.

Kinabo, B.D., Hogan, J.P., Atekwana, E.A., Abdelsalam, M.G., Modisi, M.P., 2008. Fault growth and propagation during incipient continental rifting, Insights from a combined aeromagnetic and Shuttle Radar Topography Mission digital elevation model investigation of the Okavango Rift Zone, northwest Botswana,. Tectonics 27, 1–16.

Klein, T.L., Day, W.C., 1994. Descriptive and grade-tonnage models of Archaean low-sulfide Au-quartz veins and a revised grade-tonnage model of Homestake Au, Open-file Report, United States Department of the Interior Geological Survey, page 27.

Kruse F. A., Perry, S. L., Caballero, A., 2002. Integrated multispectral and hyperspectral mineral mapping, Los Menucos, Rio Negro, Argentina, Part II, EO1 Hyperion/AVIRIS Comparisons and Landsat TM/ASTER Extensions: Jet Propulsion Laboratory Airborne Geoscience Workshop, 11th, March 2002, Proceedings, 4–8.

Kumanan, C.J., Saravanavel, J., Palanivel, K., 2011. Virues of 3D GIS in Mapping Earth-Subsurfaces Geological System/Process, ESRI Users Conference,12th, India, Proceedings, 1-5.

Loughlin, W.P., 1991. Principal component analysis for alteration mapping. Photogrammetric Eng. Remote Sens. 57, 1163–1169.

Lowman, P.D., 1991. Original shape of the Sudbury structure, Canada: a study with airborne imaging radar. Can. J. Remote Sens. 17, 152–161.

Maboko, M.A.H., 2001. The geochemistry of Banded Iron Formations in the Sukumaland Greenstone Belt of Geita, northern Tanzania: evidence for mixing of hydrothermal and clastic sources of the chemical elements. Tanzania J. Sci. 27, 21–36.

Manya, S., 2004. Geochemistry and petrogenesis of volcanic rocks of the Neoarchaean Sukumaland greenstone belt, northwestern Tanzania. J. Afr. Earth Sci. 40, 269–279.

Manya, S., Maboko, M.A.H., 2003. Dating basaltic volcanism in the Neoarchaean Sukumaland Greenstone Belt of the Tanzanian Craton using the Sm-Nd method: implications for the geological evolution of the Tanzania Craton. Precambrian Res. 121, 32–45.

Manya, S., Maboko, M.A.H., 2008. Geochemistry and geochronology of Neoarchaean volcanic rocks of the Iramba–Sekenke greenstone belt, central Tanzania. Precambrian Res. 163, 265–278.

Masoud, A.A., Koike, K., 2011. Auto-detection and integration of tectonically significant lineaments from SRTM DEM and remotely-sensed geophysical data. Int. J. Photogrammetry Remote Sens. 66, 818–832.

Maćkiewicz, A., Ratajczak, W., 1993. Principal components analysis (PCA). Comput. Geosci. 19, 303–342.

Marghany, M., Hashim, M., 2010. Lineament mapping using multispectral remote sensing data. Res. J. Appl. Sci. 5, 126–130.

McFall, G., Singhroy, V.H., 1989. Remote sensing applications to neotectonics studies in southern Ontario, Thematic Conference on Remote Sensing for Exploration Geology, Seventh, Calgary, Alberta, Canada, 1989, Proceedings, 533–546.

Naylor, W.I., 1961. Geology of the Geita district, quarter degree sheet 20 and 32. Geol. Surv. Tanganyika 9, 13–18.

Neumann, M., Ferro, L., Reigber, A., 2010. Estimation of forest structure, ground, and canopy layer characteristics from multibaseline polarimetric interferometric SAR Data. IEEE Trans. Geosci. Remote Sens. 48, 1086–1104.

Pirajno, F., 2009. Hydrothermal Processes and Mineral Systems. Springer Science and Business Media, Berlin.

Pinna, P., Muhongo, S., Mcharo, B.A., Le Goff, E., Deschamps, Y., Ralay, F., & Milesi, J.P., 2004. Geology and mineral map of Tanzania 1:2000000:Dépôtlégal 2θ trimester.

Rammlmair, D., Hdhndorf, A., Borg, G., Hiza, G.N., 1990.Nouvelles Datations Isotopiques des Granites et des Gabros de la Region 'Greenstone'-Granitique du Sukumaland, N.W.-Tanzanie, 15th Colloquium of African Geology, Nancy, Abstract Volume, 43.

Rammlmair, D., 1991. A preliminary report on the geology of the Siga Hills, NW Tanzania. Part III: Characteristics of granitoids from the Siga Hills project area. Tanzanian-German Technical Cooperation open file report, 11505/91,71.

Rowan, L.C., Mars, J.C., 2003. Lithologic mapping in the mountain pass, california, area using advanced spaceborne thermal emission and reflection radiometer (ASTER) data. Remote Sens. Environ. 84, 350–366.

Sabins, F.F., 1999. Remote sensing for mineral exploration. Ore Geol. Rev. 14, 157–183.

Sadeghi, B., Khalajmasoumi, M., Afzal, P., Moarefvand, P., Yasrebi, A.B., Wetherelt, A., Foster, P., Ziazarifi, A., 2013. Using ETM+ and ASTER sensors to identify iron occurrences in the Esfordi 1:100000 mapping sheet of Central Iran. J. Afr. Earth Sci. 85, 103–114.

Slater, J, A., Garvey, G., Johnston, C., Haase, J., Heady, B., Kroenung, G., Little, J., 2006 (The SRTM data "finishing" process and products). Photogrammetric Eng. Remote Sens. 72, 237–247.

Stanislav, I.V., Wormald, R.J., Dirks, P.H.G.M., Blenkinsop, T.G., Salamba, L., Joseph, D., 2014. Zircon U-Pb ages and Lu-Hf isotope systematics from late-tectonic granites Geita Greenstone Belt, Implications for crustal growth of the Tanzania Craton. Precambrian Res. 242, 187–204.

Stockley, 1948 (The geology and mineral resource of Tanganyika territory). Geol. Surv. Tanganyika Bull. 20, 1–37.

Vos, I.M.A., Bierlein, F.P., Standing, J.G., Davidson, G.J., 2009 (The geology and mineralization at the golden pride gold deposit, nzega greenstone belt, Tanzania). Miner. Deposita 44 (7), 751–764.

Weiser, T., 1986. Microscopic Analysis of Sulfide Associated Ores in selected Rock Samples from Gold Occurrences in the Lake Victoria Region, Tanzania, Tanzania-Germany Technical cooperation, open file report, BGR , Hannover, pp. 1-12.